Materials & Design 238 (2024) 112685

Contents lists available at ScienceDirect

Materials & Design

journal homepage: www.elsevier.com/locate/matdes

On-demand tunable metamaterials design for noise attenuation with machine learning

Lige Chang [a,b,1], Xiaowen Li [a,b,1], Zengrong Guo [a,b], Yajun Cao [a,b], Yuyang Lu [a,b], Rinaldo Garziera [c], Hanqing Jiang [a,b,d,*]

[a] School of Engineering, Westlake University, Hangzhou, Zhejiang 310030, China
[b] Westlake Institute for Advanced Study, Hangzhou, Zhejiang 310024, China
[c] Department on Engineering and Architecture, University of Parma, Parco Area delle Scienze 181/a, 43125 Parma, Italy
[d] Research Center for Industries of the Future and School of Engineering, Westlake University, Hangzhou, 310030, China

ARTICLE INFO

Keywords:
On-demand tunability
Machine learning
Acoustic metamaterial
Kresling inspired mechanical metamaterial

ABSTRACT

Metamaterials with structure-dominated properties provide a new way to design structures to obtain desired performance. To achieve a wide range of applications, on-demand tunable metamaterials would fulfill various and changing needs. The design of on-demand tunable metamaterials requires a higher-level understanding of the relationship between the properties of the metamaterials and the geometrical parameters, which in many cases are complicated and implicit. With the advancement of machine learning and evolutionary methods, it becomes possible to design on-demand tunable metamaterials. This paper designs on-demand tunable acoustic metamaterials for noise attenuation at varying frequencies by employing a genetic algorithm based neural network method. The C-shaped acoustic metamaterials with slidable shells are combined with the specifically designed tri-stable origami-inspired metamaterials to realize the on-demand tunable structure. Experiments were conducted and showed that the designed tunable metamaterials exhibited desired characteristics in different targeting frequency ranges. The present general methodology is expected to provide a route for on-demand tunable design while exploring more possibilities for the application of metamaterials.

1. Introduction

Metamaterials are structure-dominated materials with properties beyond the natural existing materials [1–5] that offer opportunities for designing new structures with uniquely desirable properties or that meet specific demands. A challenge in most metamaterials is that their properties typically remain unchanged even after fabrication [6,7], making it difficult to meet varying and various demands, which is the main limitation for the present metamaterials. To overcome this limitation, researchers have explored the use of smart materials to dynamically change the physical properties of these metamaterials under external stimuli [8–12], thus broadening the applications of metamaterials. Even more appealing, user-specific on-demand tunability offers metamaterials the ability to alter their properties based on different scenarios, thus enhancing their flexibility for various applications. The design of on-demand tunable metamaterials requires a higher-level understanding of how the properties of the metamaterials vary based on different parameters (e.g., structures or material properties) and the sensitivity of these parameters to properties.

For certain metamaterials, the relationship between the geometry parameters and physical properties can be obtained using analytical or semi-analytical means [13,14]. For example, the stiffness of a type of mechanical metamaterial, namely curved crease origami-based metamaterials, can be analytically determined based on a mathematical model [15], which enables the rapid and accurate determination of the parameters that need to be tuned for specific applications. However, for most metamaterials, their properties, such as band structures for acoustic metamaterials that relate to noise attenuation [16,17], vibration isolation [18,19], and acoustic cloaking [20,21], are usually obtained by solving a series of differential equations [22,23]. This in turn poses a challenge for correlating the property with structural parameters. Machine learning, such as neutral network methods, are considered powerful alternatives that can be used for obtaining nonlinear and implicit relationships among multiple parameters and their desired

* Corresponding author at: School of Engineering, Westlake University, Hangzhou, Zhejiang 310030, China.
E-mail address: hanqing.jiang@westlake.edu.cn (H. Jiang).
[1] These authors contributed equally.

https://doi.org/10.1016/j.matdes.2024.112685
Received 21 November 2023; Received in revised form 7 January 2024; Accepted 19 January 2024
Available online 20 January 2024

properties in complex systems [24–33] across a range of applications [34,35]. However, from a practical perspective, machine learning methods alone may not be enough for designing on-demand tunable metamaterials. This is because too many tunable geometrical parameters without any practical constraints would significantly increase the difficulty of implementation and their on-demand tunability. Therefore, for the design of on-demand metamaterials, ideally, we would like to identify one combination of a few parameters, particularly those that strongly influence the properties and form the design space. However, when these parameters are in a continuous parametric space, and not take distinct, yet discrete values, searching the entire parametric space becomes impossible; under these circumstances, evolutionary methods [36–39] seem a more appropriate solution. Finally, simple and elegant tuning mechanisms would be important to achieve practical on-demand tunable metamaterials. Since mechanical metamaterials possess characteristics to change their geometrical structure without the constraint of specific material systems, delicate structural design, with the assistance of other different metamaterials, may provide helpful solutions to achieve desired tunable functionalities.

In recent years, the design of on-demand tunable acoustic metamaterials has been highly desired (2). Acoustic metamaterials can manipulate the propagation of sound waves by designing geometry parameters [40–43], providing an effective way to attenuate the noise at target frequencies. For an example, the C-shaped structures were designed as tunable Helmholtz resonators to absorb noise at various frequencies [44–46]. Alternatively, the acoustic metamaterials with periodically distributed lattice scatters (phononic crystals) give rise to acoustic dispersions and band structures in which the acoustic waves are forbidden by the bandgaps in specific frequency spectrums [47–49]. However, the narrow width of the bandgap itself is seen as limiting its effective application range [50]. To achieve a larger effective frequency range for noise attenuation, machine learning, combined with genetic algorithm (GA), is considered an optimal approach for the design of on-demand tunable acoustic metamaterials.

In this work, we begin by stating the problems associated with on-demand tunable design as a first step to clarifying the expected performance goal. Then we move to the next step, namely, an explanation of the general data-driven methodology, including key steps, as follows: 1) determining the appropriate structure parameters, 2) constructing the neural network model using data generated from the finite element simulations, 3) performing sensitivity analysis using more data derived from the neural network model to identify key parameters with greatest influence, and 4) conducting GA to evolve to the desired metamaterials. For the implementation of the tunability, we use an origami pattern, namely Kresling-inspired mechanical metamaterials, which are designed to achieve the transformation between different structures. To verify the evolved on-demand tunable acoustic metamaterials that have our desired properties, we conducted experiments for testing acoustic performance. The results indicated that the designed tunable acoustic metamaterial achieved high-efficient noise attenuation performance for different target frequencies as expected.

2. Statement of problem

Generally, the acoustic metamaterials consisting of multiple fixed C-shaped layers (Fig. 1**a**) can only achieve acceptable noise attenuation performance at certain frequency ranges [47,48]. The cross-sectional view of the double-layer C-shaped acoustic metamaterial unit lists eight structural parameters for the outer and inner layers, including the radii R_1 and R_2, the thicknesses T_1 and T_2, the opening widths w_1 and w_2, and the rotation angles of the openings α_1 and α_2, with subscripts "1″ for outer and "2" for inner layers, respectively (Detailed diagram in Supporting Information **Fig. S1**). For the structure shown in Fig. 1**a**, finite element simulations (details in COMSOL model are provided in the **Methods** part) were conducted to calculate the transmission loss (TL) in the specific decibel values (dB) within the frequency range of 0 to 3.5

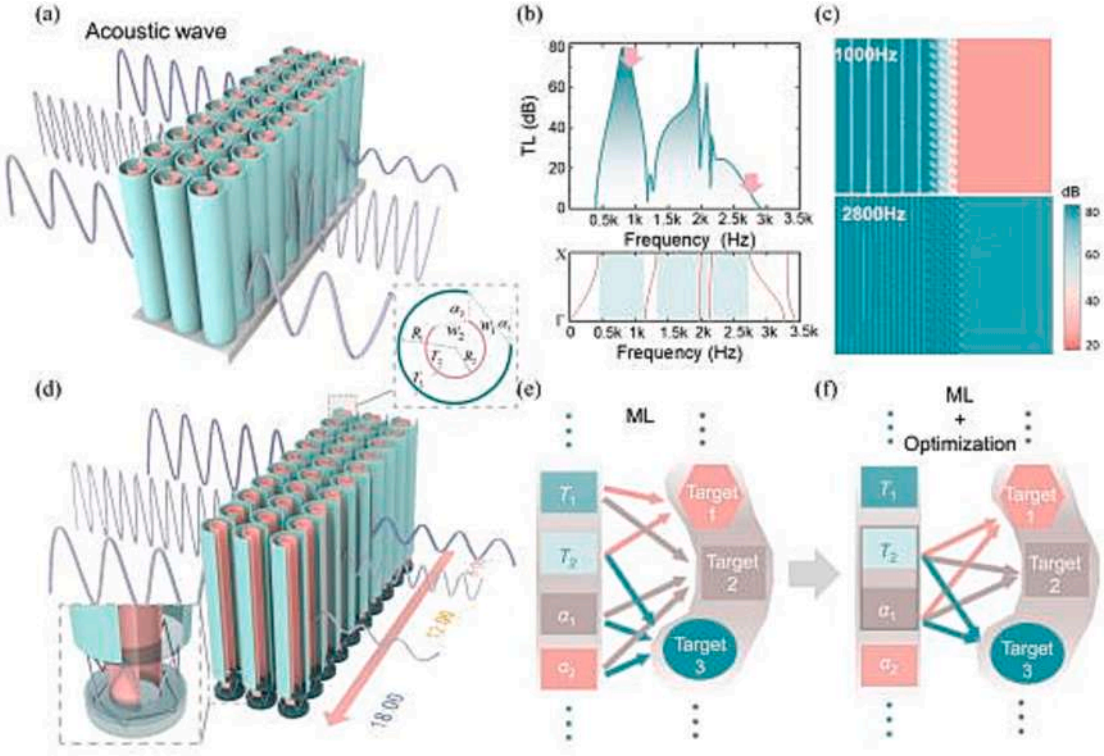

Fig. 1. Machine learning guided design of on-demand tunable acoustic metamaterials. (a) Schematic of untunable acoustic metamaterials. **(b)** The transmission loss (TL) curves and band structures for the acoustic metamaterials. **(c)** The acoustic pressure level of this acoustic metamaterial at 1,000 Hz and 2,800 Hz. **(d)** Acoustic metamaterials with the ability to tune structures with time. **(e)** Tuning all parameters to achieve different targets with ML methods. **(f)** Tuning one combination of parameters to achieve different targets with ML methods and optimization algorithm.

kHz range, as shown in the top panel of Fig. 1**b** (the material properties can be seen in **Table S1**). It is confirmed that noise attenuation is only effective within specific frequency ranges, which can be explained by the bandgap structure of a phononic crystal (bottom panel of Fig. 1**b**). Additionally, this phenomenon was corroborated by the spatial distribution of the sound pressure field, where nearly 60 dB is attenuated at 1,000 Hz and less than 10 dB is attenuated at 2,800 Hz (Fig. 1**c**), as indicated by the pink arrows in Fig. 1**b**. Furthermore, by performing additional calculations for different geometric structures, it was found that the geometries significantly influence the bandgap structure (details in **Figs. S2-S3**). The finite width of the bandgap significantly limits the frequency range for noise reduction. Given that the noise frequency always changes over time, it was expected that the acoustic metamaterials would be tuned to match the varying noises under different scenarios (Fig. 1**d**). Generally, in order to meet different targets, certain design parameters are required to be changed to cover specific frequency ranges. However, since it would be tedious (even with the machine learning (ML) method) and difficult to operate all the parameters in the practical sense (as shown in Fig. 1**e**), we hypothesized that by combining the optimization algorithms, we could achieve the same goal by simply tuning one single combination of parameters (see Fig. 1**f**). As such, this requires identifying a single combination of parameters as a first step. Once this was completed, we then focused on structural design to arrive at the intended tunable properties for enabling real-time tunability. In this work, we have employed a general data-driven methodology incorporated with GA to design a tunable acoustic metamaterial that covers broad and specific frequency ranges using band structures as the concerned property.

3. A general data-driven methodology to design acoustic metamaterials

The primary objective of this section is to establish the relationship between geometric structural parameters and noise attenuation performance, including preparation of input parameters, output parameters, and training of the neural network (NN). An important criterion is that the design of tunability needs to be balanced with the requirements of the tunable range and feasibility of implementation. To ensure convenience for installation and ventilation purposes, the radii of the outer and inner layers R_1 and R_2 are fixed, and the gaps between the neighboring metamaterial structure units are considered. The double layer C-shaped unit structure is described by six adjustable parameters, i.e., T_1, T_2, d_1, d_2, α_1, and α_2, which can be tuned through structural changes (here $d_1 = w_1/R_1$, $d_2 = w_2/R_2$, d_1 and d_2 are opening width parameters). C-shaped structures are then generated by randomly seeding between the lower and upper limits of these six parameters. Fig. 2**a** shows the distribution of the six parameters; the vertical axis is number of counts, and the total count for each parameter is 28,800, 80 % is assigned as the training set and the remaining 20 % is the testing set for the subsequent NN model. The selection of 28,800 as our dataset size is a result of careful deliberation on model performance, empirical evidence from similar studies [51], and the practicalities of computational resources. The utilization of high-quality datasets plays a crucial role in enhancing the quality of subsequent neural networks. These data are acceptably distributed within the practical ranges. Then an individual set from each parameter is randomly picked without replacement to form the corresponding acoustic metamaterial (e.g., see the star in yellow, the dot in blue and square in grey in Fig. 2**b** and their corresponding C-shaped structures); thus 28,800C-shaped structures were randomly generated. This was then followed by the generation of output data.

The band structure is a good representation to study the noise attenuation performance, given its two merits, namely low computation cost, and concise expression of the bandgap information (i.e., a starting and an ending point for one band) instead of an entire TL curve. Calculated using COMSOL Multiphysics 5.6, we obtained the band structures of 28,800C-shaped structures. Each band structure was then characterized by 10 values to describe the first five bandgaps, e.g., B_1 (starting point of the first bandgap) to B_{10} (ending point of the fifth bandgap), shown in Fig. 2**b**. An NN model containing 6 hidden layers (details in **Methods**) was then trained to reveal the relationship between the geometry parameters (a total of 6 × 28,800 data as the input layer) and bandgap structure (a total of 10 × 28,800 data as the output layer), as shown in Fig. 2**c**. To demonstrate the validity of the NN model, Fig. 2**d** shows the bandgap positions (i.e., B_1 to B_{10}) predicted by the trained NN basically collapsing with that from the finite element simulations, with average relative error of about 2.08 %, indicating trustable predictability using the trained NN model. Now the bandgaps can be predicted by the NN model once the geometry of the C-shaped acoustic metamaterials is given, which is much more efficient than the finite element simulation.

During the application process, however, tuning six parameters to match varying demands can prove to be cumbersome and even practically impossible to implement. For this reason, we employ sensitivity analysis, which helps in identifying efficient tunable parameters. Furthermore, we used generated data from the trained NN model, to conduct the sensitivity analysis [52] for identifying the most sensitive parameters among the six parameters selected. The sensitivity score is defined as [52]

$$S_i = V_{x_i}[E_{x_{\sim i}}(\boldsymbol{B}|x_i)]/V(\boldsymbol{B}) \tag{1}$$

where **B** with dimension 1 × 3,000 is a binary array, digitalizing the bandgap information from 1 to 3,000 Hz, with 1 for within a bandgap and 0 for outside of a bandgap, given a set of parameters x_i (i.e., "$|x_i$" with x_i being T_1, T_2, d_1, d_2, α_1, and α_2), $E_{x_{\sim i}}$ is the expectation over all possible values of parameters (i.e., x_i) while keeping the i^{th} parameter fixed, and V_{x_i} is the variance. The sensitivity score ranges from 0 to 1 with 1 for the strongest sensitivity. The results shown in Fig. 2**e** indicate that the opening width d_1 and the rotation angles of the openings α_1 of the outer layer have stronger effects on the bandgap position compared with the remaining four parameters. For possible values of d_1 and α_1, Fig. 2**f** shows the bandgap probability, arrived at by fixing the four parameters (T_1, T_2, d_2 and α_2) and only varying d_1 and α_1, in which one can observe that bandgaps would exist above 430 Hz with some frequencies having higher probability (e.g., close to 100 % around 1,800 Hz) and some having lower probability (e.g., about 50 % around 520 Hz).

To fully leverage the advantages of adjustable structures and enhance the noise attenuation performance, it is desirable to make appropriate structural adjustments based on the external noise using optimization algorithms. At present, GA is utilized to evolve the metamaterials by changing d_1 and α_1 to achieve the desired performance that is evaluated by the trained NN model. The performance is measured by the following fitness function,

$$f = \max\{\boldsymbol{Z}\cdot\boldsymbol{B}\}/|\boldsymbol{Z}| \tag{2}$$

where **B** is the same one-dimensional array describing the band structures for given $x_i = (d_1, \alpha_1)$, and **Z** is a one-dimensional array indicating the target noise frequency range with 0 for outside the targeted range and 1 for inside the range (Fig. 2**g**). Thus, when the fitness function f reaches 1, the bandgap would totally cover the targeted frequency range. GA is then applied to evolve the structure of the metamaterials using this fitness function f. The flowchart of this method can be found in **Fig. S4**.

4. Design and experimental verification of on-demand tunable metamaterials

Given that noise with frequencies below 3,000 Hz is one of the common types of noise in daily life [53], including traffic, mechanical and construction noise, we applied the method developed in Section 3 to design three tunable acoustic metamaterials to cover three different frequency ranges, 500 Hz to 1,400 Hz, 1,400 Hz to 2,200 Hz, and 2,200

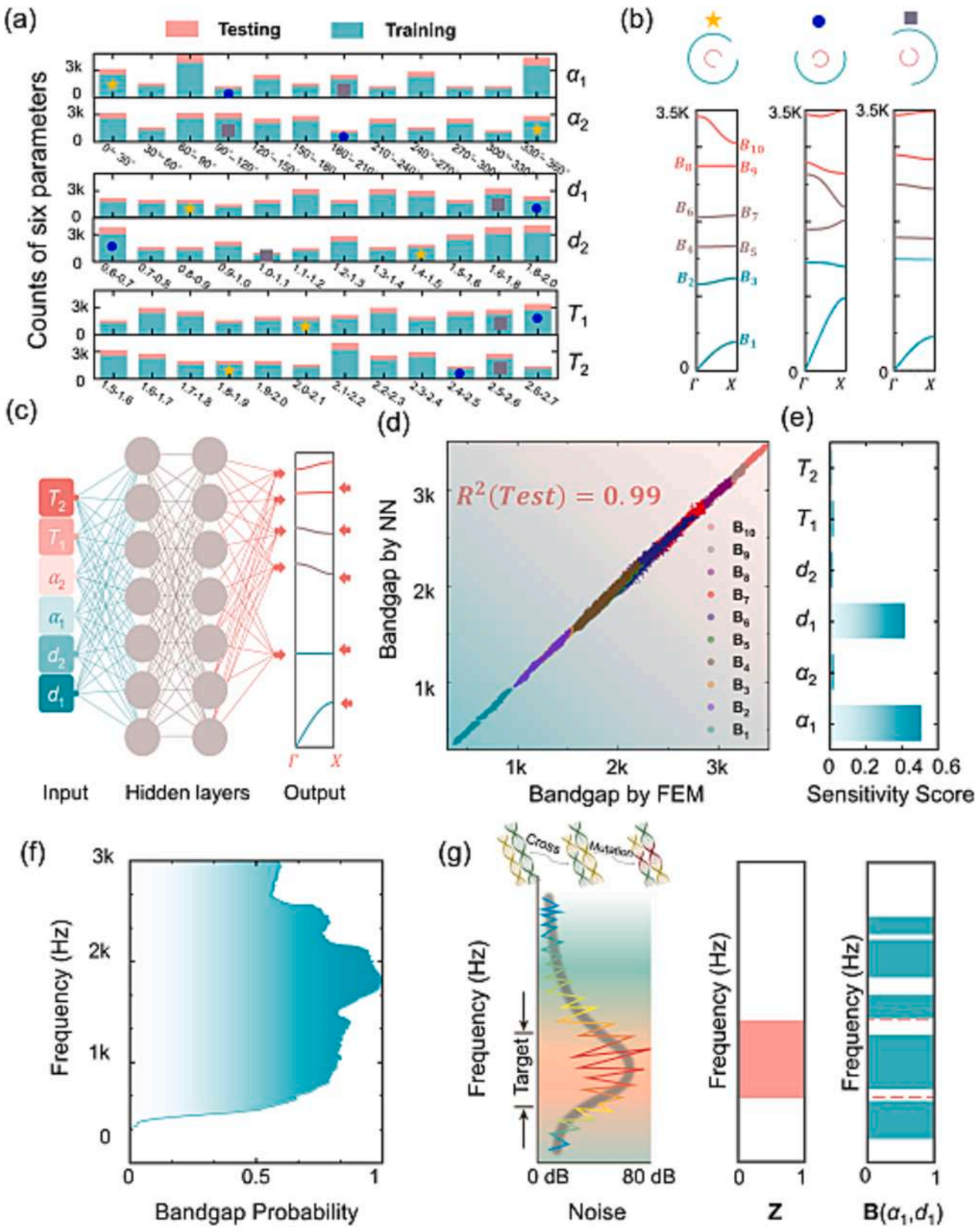

Fig. 2. Data-driven methodology to design on-demand tunable acoustic metamaterials. (a) Data preparation for α_1, α_2, d_1, d_2, T_1 and T_2. (b) The band structures for three structures. (c) The neural network used for prediction of band structures. (d) The comparison of bandgap positions between the prediction by NN and the finite element simulation. (e) Sensitivity analysis for six structural variables. (f) The bandgap probability in 0 ~ 3 k Hz range. (g) The schematic of the fitness function for GA.

Hz to 3,000 Hz, respectively. Fig. 3**a-c** show the evolution process of fitness function *f*, targeting the aforementioned three frequency ranges. The fitness function *f* reached 1 after 60 generations, indicating that the bandgaps can cover the target frequency ranges. Based on Eq. (2), the design parameters for different target frequency ranges are obtained as $\alpha_1 = 4^\circ$ and $d_1 = 1.51$, $\alpha_1 = 175^\circ$ and $d_1 = 1.95$, $\alpha_1 = 95^\circ$ and $d_1 = 0.94$ (the detailed structure parameters are given in **Table S2**) and the corresponding three optimized metamaterial units are shown in the Fig. 3**d,** which are referred as mode I, mode II and mode III. Intuitively, rotation is an efficient way to tune the structure, but it may not necessarily meet the adjustment requirements of the parameter d_1. Ideally, it is desired to find a method that only involves rotation to adjust both the opening width parameter d_1 and rotation angles of the openings α_1. Considering that the sensitivity of the layer thickness T_1 is weak, the outer layer of C-shaped structures is modified to consist of two overlapped slidable shells to realize tunability, as shown in Fig. 3**e-3f** (detailed structure of Mode I shown in **Fig. S5**). We then use finite element simulations to demonstrate that although layer thickness T_1 changes during the switching of different modes, the band structures of the original mode I structure with fixed shell (Fig. 3**d**) and the corresponding one with slidable shells (Fig. 3**e**) are almost identical (Fig. 3**g**). Additionally, the TL curves (**Fig. S6**) and acoustic pressure level results (**Fig. S7**) provide further evidence that making the optimal structures with slidable shells is reasonable.

Now we address the method of switching between different modes. In addition to using electric motors to transform among the three discrete modes, which is controlled through accurate programming, we present a novel and cost-effective solution to switch between different modes. Kresling pattern-inspired metamaterials [54,55] enable stable state transition between the deployed and collapsed states by rotating at different angles in both clockwise and counterclockwise directions. As shown in Fig. 3**h**, the shell tied on the upper panel of the Kresling-

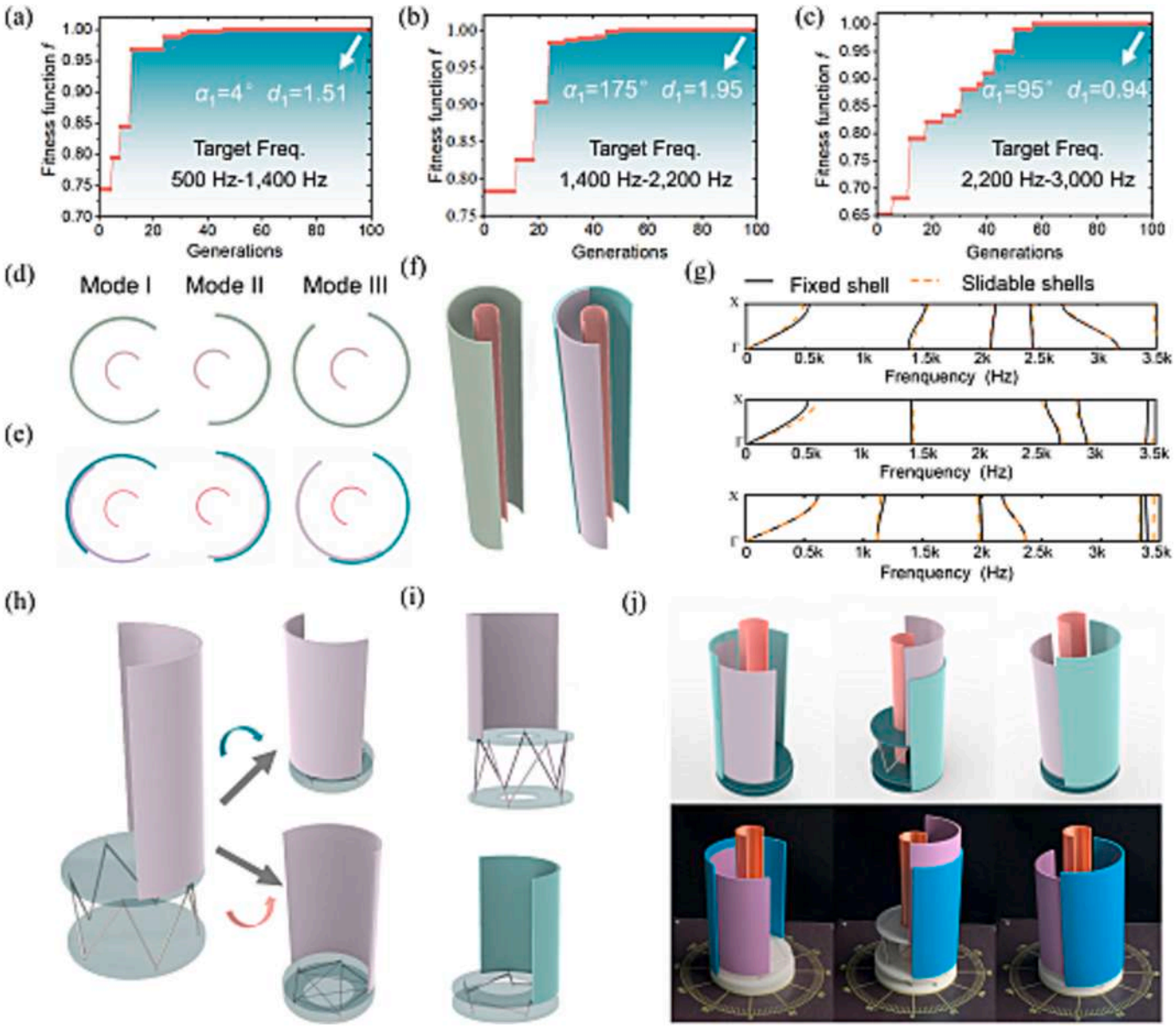

Fig. 3. The implementation of on-demand tunable acoustic metamaterials. (a)-(c) Evolution process of three metamaterial units by GA and NN. **(d)** Cross-sectional structures of optimized structures with fixed shells targeting the three frequency ranges. **(e)** Cross-sectional structures of the three modes in (d) with slidable shells. **(f)** The three-dimensional structure of metamaterial unit with fixed and slidable shells. **(g)** The band structures comparison between the modes with fixed and slidable shells. **(h)** The Kresling-inspired metamaterials can reach the collapsed state by rotating clockwise and counterclockwise. **(i)** The upper and lower Kresling-inspired metamaterials to form the transformation device. **(j)** The three modes realized by the transformation devices.

inspired truss structure can transfer to different positions when the panel is rotated clockwise (blue arrow) and counterclockwise (red arrow) directions. Therefore, each of the Kresling-inspired structures have three stable states, one for deployed state and two for collapsed states by rotating clockwise and counterclockwise. As shown in Fig. 3**i**, there are two Kresling pattern-inspired truss structures with the top one controlling one sliding outer layer and the bottom for another sliding outer layer. By employing two tri-table Kresling pattern-inspired structures to control the two sliding shells on the outer layer, we are able to achieve transition among three states. Thus, by properly designing the parameters of the Kresling-inspired structures, transformation takes place from mode II to mode I, and mode II to mode III. The detailed design, parameters, and components for building the Kresling pattern-inspired truss structures are provided in supporting information (**Figs. S8-S9**, **Table S3-S5**). By clockwise rotating both the top and bottom Kresling-inspired structures by 116° and 22°, respectively, mode II (Fig. 3**j**, *middle*) transfers to mode I (Fig. 3**j**, *left*). This process can be seen in **Movie S1**. Through counterclockwise rotation of the top and bottom Kresling-inspired structures by 89° and 134°, respectively, mode II transfers to mode III (Fig. 3**j**, *right*), shown in **Movie S2**.

To verify the noise attenuation performance at targeted frequency ranges, acoustic testing was conducted. The photograph of the experiment setup is shown in Fig. 4**a** (details in **Methods**). The acoustic metamaterials measure 1.8 m in height and are placed in the middle of a semi-anechoic chamber. The acoustic signals were measured for different modes, and the TL curves were plotted shown in Fig. 4**b to 4d**. The sound in the targeted frequency ranges were selectively attenuated, for the purpose of verifying that the designed acoustic metamaterials achieve on-demand tunability by sliding the shells. The trends of the TL curves for both the simulations and experiments also coalesce very well. Discrepancy between experiments and simulations may occur due to factors, such as manufacturing errors and slight differences in experimental setup and two-dimensional simulation models. The effective TL between frequencies f_1 and f_2 defined as [7] $\int_{f_1}^{f} TLdf/(f_2 - f_1)$ is used to quantify the acoustic performance. As shown in Fig. 4**e**, as the design expects, mode I has the highest effective TL of between 500 Hz and 1,400 Hz (i.e., 33.4 dB for simulation and 26.6 dB for experiment as indicated in blue arrows), closely followed by mode II, which has the highest effective TL for its desired frequency range, and mode III, which prevails over the other two modes, ranging between 2,200 Hz to 3,000 Hz. During the installation of our system, a gap is likely to form between the fixed shell and the slidable shell. To understand how this gap affects noise attenuation, we conducted simulations to analyze the transmission loss curve with the presence of a gap in three different modes. The outcomes of these simulations are depicted in **Fig. S10**. Our findings suggest that the gap between the fixed and slidable shells has a marginal impact on the system's noise attenuation performance.

5. The extensibility of tunable acoustic metamaterials.

The selected three acoustic metamaterials can be placed in series to cover a wide and tunable frequency range for noise attenuation. The noise attenuation performance of the combination of the two modes is shown in Fig. 5. The photographic experimental setups are shown in Fig. 5**a.** To verify their performance, the transmission loss was simulated and experimentally measured using modes I and II with three layers each (see the planar layout of this combination in Fig. 5**b**). The results (Fig. 5**c**) clearly show that TL in the desired frequency range is enhanced, with effective TL of 33 dB for experiments, compared with that for the individual modes, i.e., 26.6 dB (mode I) and 18.39 dB (mode II) for 500 Hz to 1,400 Hz, and 24.8 dB (mode I) and 28.6 dB (mode II) for 1,400 Hz to 2,200 Hz. Fig. 5**f** is the simulated acoustic pressure level for mode I and mode II combinations at 700 Hz and 2,200 Hz. Similar combinations can be performed for modes II and III to cover higher frequency ranges (Fig. 5**d, 5e and 5 g**). It should be emphasized that since these acoustic metamaterials are tunable, modes I, II, and III are interchangeable by simply sliding the shells. Depending on the application scenario, these metamaterials can be tuned for a narrow range (i.e., individual modes) or a combined range (i.e., mixed modes), which then fully utilizes the merit of being readily tunable. Since the Kresling-based tunable system at the bottom of the C-shaped structure are mainly made of rods that would allow for the sound wave propagation when this structure is deployed, to decouple this effect from the acoustic performance, we didn't include the Kresling-based tunable system in the acoustic test. For practical applications, Kresling-inspired units would be encapsulated in customized boxes at the bottom of the sound barrier, which will not compromise the noise attenuation performance of the sound barrier.

In addition, there still needs many efforts to explore a stable and low-cost driving method to operate the Kresling-inspired structure. A promising method involves integrating airbags within the Kresling-inspired unit. Controlling the amount of air inflation and deflation can trigger the switching between different modes. This method is cost-effective, but facing the synchronization problem due to the pneumatic delay, which is suitable to the application scenarios where the frequency range of external noise changes slowly. In this case, the requirement for synchronization in the sound barrier is relatively low. When the frequency range of external noise changes quickly, the electric motor can be used for each Kresling-inspired unit, achieving synchronized adjustments becomes possible.

6. Conclusion

In this study, we presented an NN combined with GA-based method to design on-demand C-shaped tunable acoustic metamaterials for noise attenuation. The relationship between geometric dimensions and bandgap was determined using NN. Using parameter sensitivity analysis, we identified that the opening width and rotation angles of the openings were critical factors, and by manipulating their combination we can attenuate noise with different frequencies. By combining NN with GA, the structures of the acoustic metamaterials corresponding to different given frequency ranges were also determined. Three modes were identified for three frequency ranges. Furthermore, slidable shells were designed for the outer layer of the C-shaped tunable acoustic metamaterials, and a Kresling-inspired mechanical metamaterial with a tri-stable state was developed to control rotation and enable switching among three modes, thereby achieving noise attenuation at various frequencies. The designed tunable acoustic metamaterials were validated through experimental measurements showing good agreement between theory and practice. It is thus believed that the present general methodology would provide a route for well-regulated on-demand tunable design. Furthermore, its integration with other active components and controls would lead to new engineering improvements.

7. Methods

Experimental setup: 3 × 16 units (3 rows, each row with 16 units) are arranged to measure the acoustic attenuation performance. The metamaterials are fabricated by PVC pipes. The size of each unit is 100 mm (length) × *l*00 mm (width) × 1,800 mm (height). The power amplifier (Sound Blaster X7, Creative) was used to amplify the input signal. The loud speaker (HI-VIRESEARC W11905472, HiVi Acoustics Inc.) was connected to convert the electrical signals into acoustic signals. The microphone (AWA14423, HangZhou Aihua Instruments Co., Ltd) is able to detect the acoustic signals with an open circuit sensitivity of 48.97 mV/Pa. The sound source is white noise. The acoustic experiment was conducted in a semi-anechoic chamber. The distance between the acoustic source and the acoustic metamaterials was 0.7 m, and the distance between the microphone and the acoustic metamaterials was 0.7 m.

Rationales of the selection of six parameters:

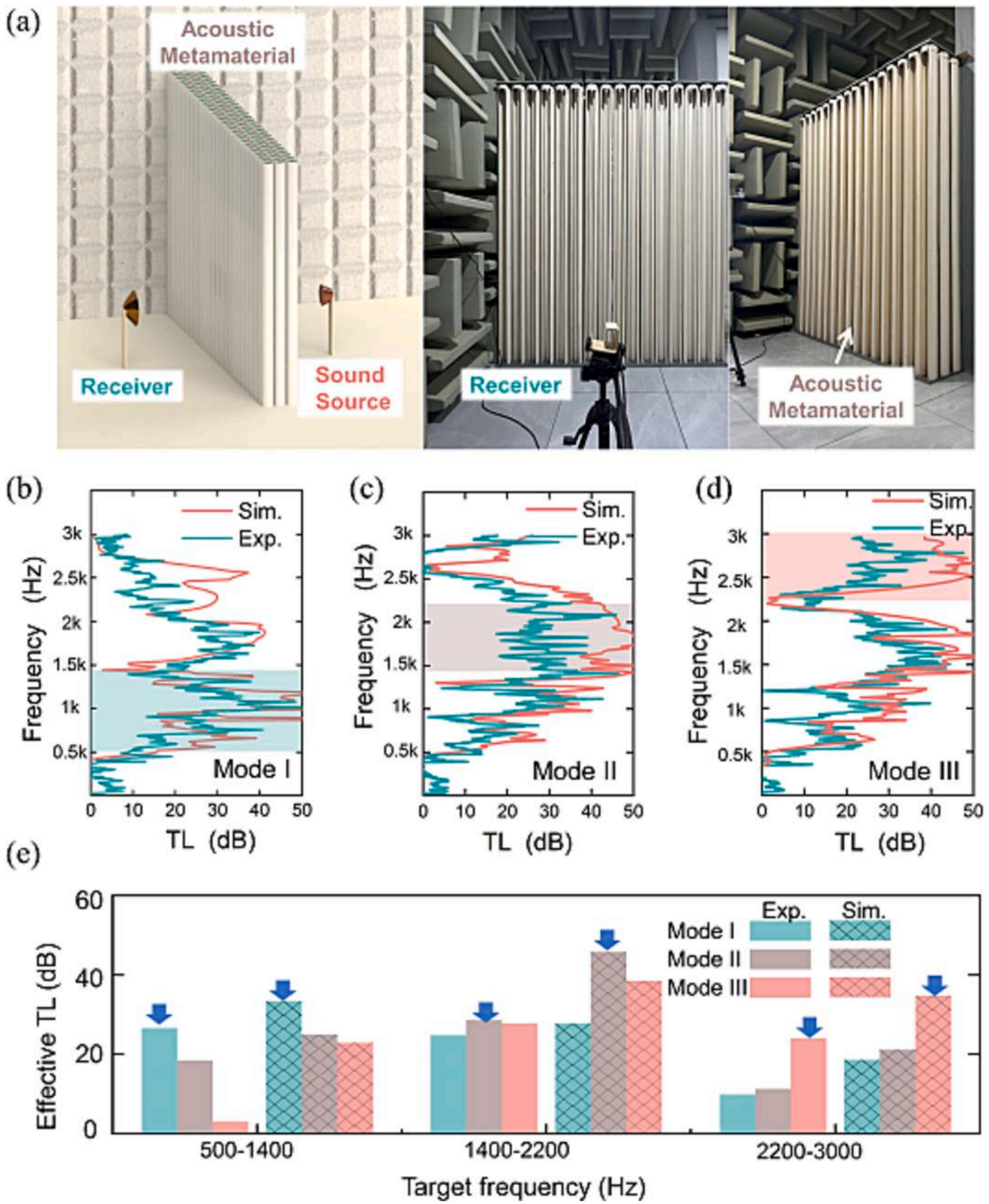

Fig. 4. Experimental verification of on-demand tunable acoustic metamaterials. (a) The experiment setup. (b)-(d) The experimental measurements and simulations of TL curves for mode I, mode II, and mode III. (e) The calculating effective TL from experimental and simulated data for three modes under three targeted frequencies.

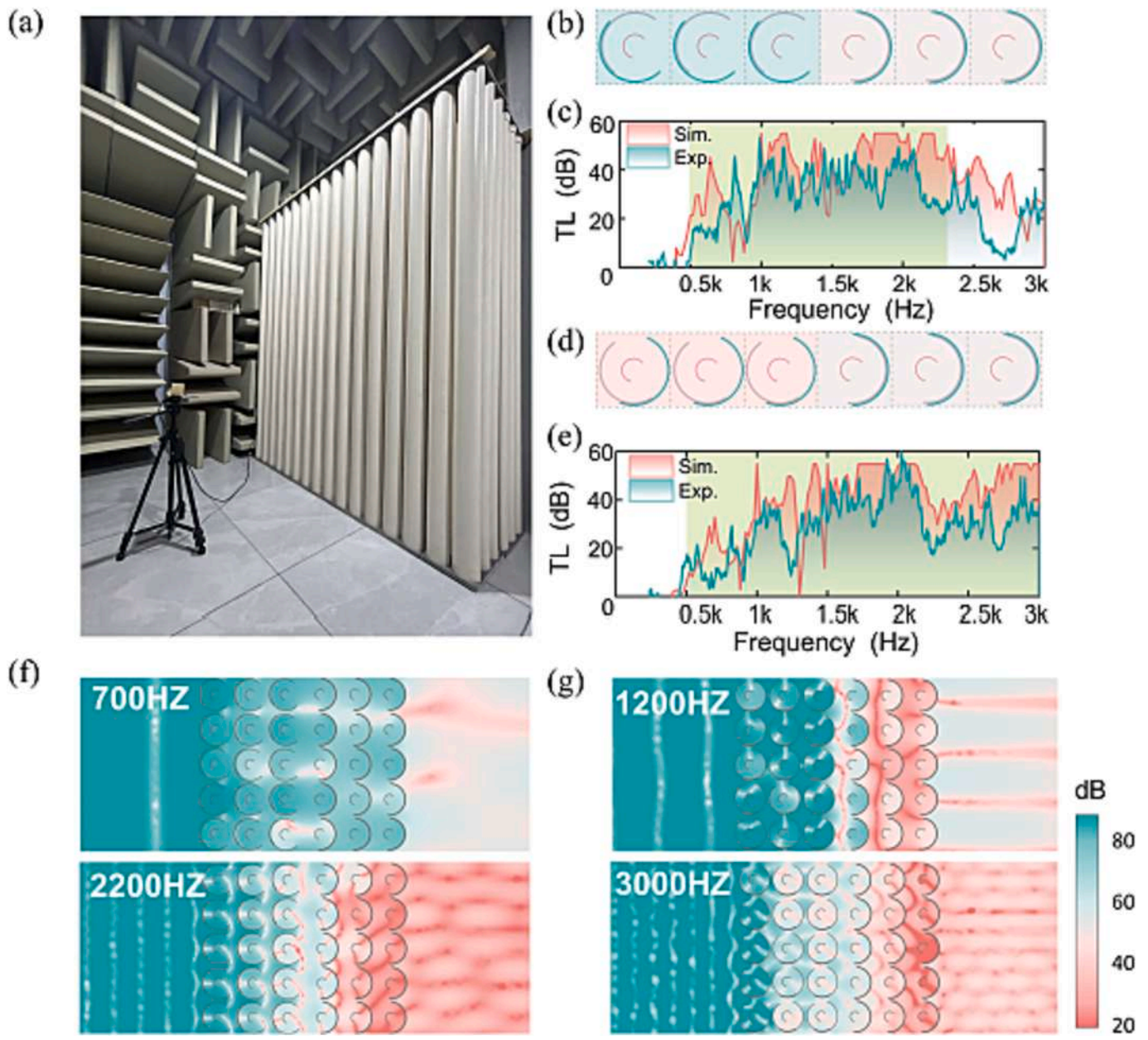

Fig. 5. Noise attenuation performance of two-modes combination. (a) Photographic experiment setups. (b) Planar layout of combination of mode I and Mode II. (c) The TL curves of combination of mode I and mode II. (d) Planar layout of combination of mode III and mode II. (e) The TL curves of combination of mode III and mode II. (f) Simulated acoustic pressure level for combination of mode I and mode II at 700 Hz and 2,200 Hz. (g) Simulated acoustic pressure level for combination of mode III and mode II at 1,200 Hz and 3,000 Hz.

The lower and upper limits of the six parameters ($\alpha 1$, $\alpha 2$, T_1, T_2, d_1, d_2) are mainly determined by the application requirements and material processing:

(1) The selection for the opening angle (α_1, α_2) ranges from 0 to 360 degrees to cover the entire circumference.
(2) The selection of the thickness for the C-shaped shell (T_1, T_2) balances overall weight and structural stability. For a sound barrier standing 1.8 m tall, using very thin C-shaped shells could compromise stability, especially during movement. Conversely, shells that are too thick would significantly increase the overall weight, making it challenging to adjust and tune the structure effectively. We found that a shell thickness ranging between 1.5 mm and 2.7 mm offers an optimal balance, providing both stability and ease of tuning in our experiments. Additionally, we opted for PVC pipes to fabricate these C-shaped shells, as PVC pipes within this thickness range are readily available in the market. This choice not only meets our structural requirements but also helps in reducing the experimental costs.
(3) The ranges for the opening width parameters (d_1, d_2) are set between 0.6 and 2.0, with the corresponding opening central angles ranging from 35° to 180°. This design consideration is twofold. Firstly, it is essential to keep the central angle of the opening below 180°. Doing so ensures the formation of an effective cavity that is conducive to noise absorption. Secondly, the minimum central angle is set above 35°, taking into account practical aspects such as the ease of installation and operational efficiency during sample fabrication. These parameters are carefully chosen to optimize the structural design for maximum noise absorption while maintaining practicality in construction and use.

Details in the COMSOL model:

The COMSOL model schematic is shown in Fig. S11. In Fig. S11**a**, the computational model for the bandgap structure is depicted, utilizing the Pressure Acoustics physical field and the Frequency Domain module for an eigenfrequency study. Considering only vertically incident noise on the sound barrier, periodic boundary conditions are applied to boundaries B and D, while continuous boundary conditions are set for boundaries A and C. Fig. S11**b** illustrates the model employed for calculating transmission loss. It also utilizes the Pressure Acoustics and Frequency Domain modules, focusing on frequency domain analysis. To closely replicate the experimental setup, a grid comprising 3 × 16 structural units is used. The yellow region in the model represents the background pressure field, while the purple region denotes the perfectly matched layer (PML). The PML is crucial as it simulates a non-reflecting infinite domain, with its external boundary acting as a sound hard boundary. The specific model parameters employed in these simulations are detailed in Table S1.

Construction of NN model: The fully connected neural network (NN) contains one input layer, six hidden layers and one output layer. The training process of the NN was implemented using TensorFlow (v2.10.0). The number of neuron nodes of the six hidden layers was set as 2^n, with n = 4 to 9 (the node number for the first hidden layer was 2^4, for the second hidden layer was 2^5…for the sixth hidden layer was 2^9). Because the input layer has 6 nodes and the output layer has 10 nodes, there are 1,024 learnable parameters for the NN training in total. The ReLU (Rectified Linear Unit) activation function for the hidden layers was applied to introduce nonlinearity. For the output layer, since the results of the physical problems in this study are non-negative, the ReLU activation function was employed to obtain the predicted outcomes. We used the TensorFlow (v2.11.0) framework to implement the NN model. To evaluate the discrepancy between the model's predictions and the actual values, mean squared error (MSE) was used as the loss function. The Adam optimizer with adaptive learning rate was selected as the optimizer. The NN was trained based on a CPU core (Intel Core i9-12900 KS) and a GPU (NVIDIA GeForce RTX 3080 Ti), which took 27.6 mins.

Methods for GA optimization: The population was set at 30 for each generation, which means the NN would be invoked 30 times for predicting the band structures for each generation. Starting from a generation containing randomly selected 30 individuals, each individual was evaluated by the fitness function and then underwent crossover and mutation. The evolution process of GA stopped when the generations reached 100. The crossover fraction was set as 0.9 and the mutation probability was 0.1. The GA optimization process was performed by Python 3.10.

Design and fabrication of the transformation device of the three modes: Two Kresling-inspired metamaterials were combined together to achieve the rotation of the two shells of the outer layer. Each Kresling-inspired metamaterial consisted of two panels (upper panel and lower panel), 10 hollow pillars, and elastic strings. The panels were made of PLA using 3D printing. The hollow pillars were fabricated with stainless steel with a diameter of two millimeters; elastic strings were put inside the hollow pillars to connect the upper and lower panels.

CRediT authorship contribution statement

Lige Chang: Writing – review & editing, Writing – original draft, Software, Methodology, Investigation, Conceptualization. **Xiaowen Li:** Software, Methodology, Data curation. **Zengrong Guo:** Software, Methodology. **Yajun Cao:** Writing – original draft, Methodology. **Yuyang Lu:** Writing – review & editing, Writing – original draft, Methodology, Funding acquisition, Conceptualization. **Rinaldo Garziera:** Software, Methodology, Conceptualization. **Hanqing Jiang:** Writing – review & editing, Writing – original draft, Visualization, Resources, Funding acquisition.

Declaration of competing interest

The authors declare that they have no known competing financial interests or personal relationships that could have appeared to influence the work reported in this paper.

Data availability

Data will be made available on request.

Acknowledgements

We thank the Research Center for Industries of the Future (RCIF) at Westlake University and Westlake Education Foundation for supporting this work. L.C. acknowledges support from the China Postdoctoral Science Foundation (Grants 2022M722837). Y.L. acknowledges support from the National Natural Science Foundations of China (Grants No. 12202366). H.J. acknowledges support from the National Natural Science Foundations of China (Grants 12350003).

Appendix A. Supplementary data

Supplementary data to this article can be found online at https://doi.org/10.1016/j.matdes.2024.112685.

References

[1] C. Lu, M. Hsieh, Z. Huang, C. Zhang, Y. Lin, Q. Shen, F. Chen, L. Zhang, Architectural design and additive manufacturing of mechanical metamaterials: a review, Engineering 17 (2022) 44–63, https://doi.org/10.1016/j.eng.2021.12.023.

[2] S.A. Cummer, J. Christensen, A. Alù, Controlling sound with acoustic metamaterials, Nat. Reviews Mater. 1 (3) (2016), https://doi.org/10.1038/natrevmats.2016.1.

[3] N. Gao, Z. Zhang, J. Deng, X. Guo, B. Cheng, H. Hou, Acoustic Metamaterials for Noise Reduction: A Review, Adv. Mater. Technol. 7 (6) (2022) 2100698, https://doi.org/10.1002/admt.202100698.

[4] G. Liao, C. Luan, Z. Wang, J. Liu, X. Yao, J. Fu, Acoustic Metamaterials: A Review of Theories, Structures, Fabrication Approaches, and Applications, Adv. Mater. Technol. 6 (5) (2021) 2000787, https://doi.org/10.1002/admt.202000787.

[5] G. Ji, J. Huber, Recent progress in acoustic metamaterials and active piezoelectric acoustic metamaterials - A review, Appl. Mater. Today 26 (2022) 101260, https://doi.org/10.1016/j.apmt.2021.101260.

[6] M. Kadic, G.W. Milton, M. van Hecke, M. Wegener, 3D metamaterials, Nat. Reviews Phys. 1 (3) (2019) 198–210, https://doi.org/10.1038/s42254-018-0018-y.

[7] L. Wu, Z. Zhai, X. Zhao, X. Tian, D. Li, Q. Wang, H. Jiang, Modular Design for Acoustic Metamaterials: Low-Frequency Noise Attenuation, Adv. Funct. Mater. (2021) 2105712, https://doi.org/10.1002/adfm.202105712.

[8] S.M. Montgomery, S. Wu, X. Kuang, C.D. Armstrong, C. Zemelka, Q. Ze, R. Zhang, R. Zhao, H.J. Qi, Magneto-Mechanical Metamaterials with Widely Tunable Mechanical Properties and Acoustic Bandgaps, Adv. Funct. Mater. 31 (3) (2020) 2005319, https://doi.org/10.1002/adfm.202005319.

[9] T.D. Filippo Casadei, A. Bergamini, P. Ermanni, Massimo Ruzzene, Piezoelectric resonator arrays for tunable acoustic waveguides and metamaterials, J. Appl. Phys. 112 (2012), https://doi.org/10.1063/1.4752468.

[10] C.-M.-C. Christina, J. Naify, G. McKnight, S. Nutt, Transmission loss of membrane-type acoustic metamaterials with coaxial ring masses, J. Appl. Phys. 110 (2011), https://doi.org/10.1063/1.3665213.

[11] Z. Xiao, P. Gao, X. He, Y. Qu, L. Wu, Multifunctional acoustic metamaterial for air ventilation, broadband sound insulation and switchable transmission, J. Phys. D: Appl. Phys. 56 (4) (2022) 044006, https://doi.org/10.1088/1361-6463/acaa44.

[12] Z. Xiao, P. Gao, D. Wang, X. He, L. Wu, Ventilated metamaterials for broadband sound insulation and tunable transmission at low frequency, Extreme Mech. Lett. 46 (2021), https://doi.org/10.1016/j.eml.2021.101348.

[13] W. Wu, R. Xia, G. Qian, Z. Liu, J. Razavi, F. Berto, H. Gao, Mechanostructures: Rational mechanical design, fabrication, performance evaluation, and industrial application of advanced structures, Prog. Mater. Sci. 131 (2023), https://doi.org/10.1016/j.pmatsci.2022.101021.

[14] Y. Yao, Y. Ni, L.H. He, Rutile-mimic 3D metamaterials with simultaneously negative Poisson's ratio and negative compressibility, Mater. Des. 200 (2021), https://doi.org/10.1016/j.matdes.2020.109440.

[15] Z. Zhai, Y. Wang, K. Lin, L. Wu, H. Jiang, In situ stiffness manipulation using elegant curved origami, Sci. Adv. (2020), https://doi.org/10.1126/sciadv.abe2000.

[16] S. Li, Y. Dou, T. Chen, J. Xu, B. Li, F. Zhang, Designing a broad locally-resonant bandgap in a phononic crystals, Phys. Lett. A 383 (12) (2019) 1371–1377, https://doi.org/10.1016/j.physleta.2019.01.061.

[17] J. Radosz, Acoustic performance of noise barrier based on sonic crystals with resonant elements, Appl. Acoust. 155 (2019) 492–499, https://doi.org/10.1016/j.apacoust.2019.06.003.
[18] H. Liu, Q. Zhang, K. Zhang, G. Hu, H. Duan, Designing 3D Digital Metamaterial for Elastic Waves: From Elastic Wave Polarizer to Vibration Control, Adv. Sci. 6 (16) (2019) 1900401, https://doi.org/10.1002/advs.201900401.
[19] F. Yang, J.-S. Yang, Y. Wang, S. Li, M.-G. Zhang, R. Schmidt, K.-U. Schröder, Theoretical study on dispersion relations of chiral acoustic metamaterials considering mass-rotation, Eur. J. Mech. - A/solids 100 (2023), https://doi.org/10.1016/j.euromechsol.2023.105005.
[20] A. Colombi, P. Roux, S. Guenneau, M. Rupin, Directional cloaking of flexural waves in a plate with a locally resonant metamaterial, J. Acoust. Soc. Am. 137 (4) (2015) 1783–1789, https://doi.org/10.1121/1.4915004.
[21] Y. Huang, X. Lu, G. Liang, Z. Xu, Pentamodal property and acoustic band gaps of pentamode metamaterials with different cross-section shapes, Phys. Lett. A 380 (13) (2016) 1334–1338, https://doi.org/10.1016/j.physleta.2016.01.041.
[22] M.S. Kushwaha, P. Halevi, G. Martinez, L. Dobrzynski, B. Djafari-Rouhani, Theory of acoustic band structure of periodic elastic composites, Phys. Rev. B 49 (4) (1994) 2313–2322, https://doi.org/10.1103/physrevb.49.2313.
[23] P. Gao, A. Climente, J. Sánchez-Dehesa, L. Wu, Single-phase metamaterial plates for broadband vibration suppression at low frequencies, J. Sound Vib. 444 (2019) 108–126, https://doi.org/10.1016/j.jsv.2018.12.022.
[24] C. Kim, R. Batra, L. Chen, H. Tran, R. Ramprasad, Polymer design using genetic algorithm and machine learning, Comp. Mater. Sci. 186 (2021) 110067, https://doi.org/10.1016/j.commatsci.2020.110067.
[25] F. Liu, X. Jiang, X. Wang, L. Wang, Machine learning-based design and optimization of curved beams for multistable structures and metamaterials, Extreme Mech. Lett. 41 (2020) 101002, https://doi.org/10.1016/j.eml.2020.101002.
[26] K. Guo, Z. Yang, C.-H. Yu, M.J. Buehler, Artificial intelligence and machine learning in design of mechanical materials, Mater. Horizons 8 (4) (2021) 1153–1172, https://doi.org/10.1039/d0mh01451f.
[27] M.A. Bessa, P. Glowacki, M. Houlder, Bayesian Machine Learning in Metamaterial Design: Fragile Becomes Supercompressible, Adv. Mater. 31 (48) (2019) e1904845.
[28] C. Wang, H. Fu, L. Jiang, D. Xue, J. Xie, A property-oriented design strategy for high performance copper alloys via machine learning, npj Comput, Mater. 5 (2019) 1–8, https://doi.org/10.1038/s41524-019-0227-7.
[29] G.M. Coli, E. Boattini, L. Filion, M. Dijkstra, Inverse design of soft materials via a deep learning–based evolutionary strategy, Sci. Adv. (2022), https://doi.org/10.1126/sciadv.abj6731.
[30] R. Guo, Y. Fang, Z. Wang, A. Libanori, X. Xiao, D. Wan, X. Cui, S. Sang, W. Zhang, H. Zhang, J. Chen, Deep learning assisted body area triboelectric hydrogel sensor network for infant care, Adv Funct. Mater. (2022) 2204803, https://doi.org/10.1002/adfm.202204803.
[31] T.W. Liu, C.T. Chan, R.T. Wu, Deep-Learning-Based Acoustic Metamaterial Design for Attenuating Structure-Borne Noise in Auditory Frequency Bands, Mater. 16 (5) (2023), https://doi.org/10.3390/ma16051879.
[32] M. Fathidoost, Y. Yang, M. Oechsner, B.-X. Xu, Data-driven thermal and percolation analyses of 3D composite structures with interface resistance, Mater. Des. 227 (2023) 111746, https://doi.org/10.1016/j.matdes.2023.111746.
[33] H. Zhang, Y. Wang, H. Zhao, K. Lu, D. Yu, J. Wen, Accelerated topological design of metaporous materials of broadband sound absorption performance by generative adversarial networks, Mater. Des. 207 (2021) 109855, https://doi.org/10.1016/j.matdes.2021.109855.
[34] T.-W. Rih-Teng Wu, M.R. Liu, Jahanshahi, Fabio Semperlotti. Design of one-dimensional acoustic metamaterials using machine learning and cell concatenation, Struct. Multidiscipl. Optim. (2021), https://doi.org/10.1007/s00158-020-02819-6.
[35] A. Bacigalupo, G. Gnecco, M. Lepidi, L. Gambarotta, Machine-learning techniques for the optimal design of acoustic metamaterials, J. Optim. Theory Appl. 187 (3) (2019) 630–653, https://doi.org/10.1007/s10957-019-01614-8.
[36] L. Wu, L. Liu, Y. Wang, Z. Zhai, H. Zhuang, D. Krishnaraju, Q. Wang, H. Jiang, A machine learning-based method to design modular metamaterials, Extreme Mech. Lett. 36 (2020) 100657, https://doi.org/10.1016/j.eml.2020.100657.
[37] X. He, H.-W. Dong, Z. Ren, S.-D. Zhao, K. Wang, Y. Hu, P. Xiang, Y. Li, M. Chen, D. Fang, Inverse-designed single-phase elastic metasurfaces for underwater acoustic vortex beams, J. Mech. Phys. Solids 174 (2023), https://doi.org/10.1016/j.jmps.2023.105247.
[38] Z. Liu, H.-W. Dong, G.-L. Yu, L. Cheng, Achieving ultra-broadband and ultra-low-frequency surface wave bandgaps in seismic metamaterials through topology optimization, Compos. Struct. 295 (2022), https://doi.org/10.1016/j.compstruct.2022.115863.
[39] D.F. Cook, C.T. Ragasdale, R.L. Major, Combining a neural network with a genetic algorithm for process parameter optimization, Eng. Appl. Artif. Intell. 13 (2000).
[40] N. Gao, H. Yu, J. Liu, J. Deng, Q. Huang, D. Chen, G. Pan, Experimental investigation of composite metamaterial for underwater sound absorption, Appl. Acoust. 211 (2023), https://doi.org/10.1016/j.apacoust.2023.109466.
[41] N. Gao, J. Wu, K. Lu, H. Zhong, Hybrid composite meta-porous structure for improving and broadening sound absorption, Mech. Syst. Signal Process. 154 (2021), https://doi.org/10.1016/j.ymssp.2020.107504.
[42] Z. Zhou, S. Huang, D. Li, J. Zhu, Y. Li, Broadband impedance modulation via non-local acoustic metamaterials, Natl. Sci. Rev. 9 (8) (2022), https://doi.org/10.1093/nsr/nwab171.
[43] M. Yang, S. Chen, C. Fu, P. Sheng, Optimal sound-absorbing structures, Mater. Horizons 4 (4) (2017) 673–680, https://doi.org/10.1039/c7mh00129k.
[44] Z.-X. Xu, H.-Y. Meng, A. Chen, J. Yang, B. Liang, J.-C. Cheng, Tunable low-frequency and broadband acoustic metamaterial absorber, J. Appl. Phys. 129 (9) (2021), https://doi.org/10.1063/5.0038940.
[45] X. Wu, C. Fu, X. Li, Y. Meng, Y. Gao, J. Tian, L. Wang, Y. Huang, Z. Yang, W. Wen, Low-frequency tunable acoustic absorber based on split tube resonators, Appl. Phys. Lett. 109 (4) (2016), https://doi.org/10.1063/1.4959959.
[46] A. Chen, Z.-X. Xu, B. Zheng, J. Yang, B. Liang, J.-C. Cheng, Machine learning-assisted low-frequency and broadband sound absorber with coherently coupled weak resonances, Appl. Phys. Lett. 120 (3) (2022), https://doi.org/10.1063/5.0071036.
[47] D.P. Elford, L. Chalmers, F.V. Kusmartsev, G.M. Swallowe, Matryoshka locally resonant sonic crystal, J. Acoust. Soc. Am. 130 (5) (2011) 2746–2755, https://doi.org/10.1121/1.3643818.
[48] X. Hu, C.T. Chan, J. Zi, Two-dimensional sonic crystals with Helmholtz resonators, Phys. Rev. E. 71 (5 Pt 2) (2005) 055601, https://doi.org/10.1103/PhysRevE.71.055601.
[49] K.H. Matlack, A. Bauhofer, S. Krödel, A. Palermo, C. Daraio, Composite 3D-printed metastructures for low-frequency and broadband vibration absorption, Proc. Natl. Acad. Sci. 113 (30) (2016) 8386–8390, https://doi.org/10.1073/pnas.1600171113.
[50] S. Ning, F. Yang, C. Luo, Z. Liu, Z. Zhuang, Low-frequency tunable locally resonant band gaps in acoustic metamaterials through large deformation, Extreme Mech. Lett. 35 (2020) 100623, https://doi.org/10.1016/j.eml.2019.100623.
[51] B. Deng, A. Zareei, X. Ding, J.C. Weaver, C.H. Rycroft, K. Bertoldi, Inverse design of mechanical metamaterials with target nonlinear response via a neural accelerated evolution strategy, Adv. Mater. 34 (41) (2022) 2206238, https://doi.org/10.1002/adma.202206238.
[52] A. Saltelli, P. Annoni, I. Azzini, F. Campolongo, M. Ratto, S. Tarantola, Variance based sensitivity analysis of model output. Design and estimator for the total sensitivity index, Comput. Phys. Commun. 181(2) (2010) 259-270. doi: 10.1016/j.cpc.2009.09.018.
[53] S. U, The multi-coincidence peak around 1000 Hz in tyre/road noise spectra, Euronoise Naples 89 (2003) 1-8.
[54] C. Jianguo, D. Xiaowei, Z. Ya, F. Jian, T. Yongming, Bistable Behavior of the Cylindrical Origami Structure With Kresling Pattern, J. Mech. Design 137 (6) (2015), https://doi.org/10.1115/1.4030158.
[55] Z. Zhai, Y. Wang, H. Jiang, Origami-inspired, on-demand deployable and collapsible mechanical metamaterials with tunable stiffness, Proc. Natl. Acad. Sci. s 115 (9) (2018), https://doi.org/10.1073/pnas.1720171115.